Journal of Nonlinear and Convex Analysis
Volume 26, Number 10, 2025, 2929–2942

Yokohama Publishers
ISSN 1880-5221 ONLINE JOURNAL

AN ANALYSIS ON GENERATING JULIA AND MANDELBROT SETS USING THE W-ITERATION SCHEME WITH NUMERICAL RESULTS

NABARAJ ADHIKARI AND WUTIPHOL SINTUNAVARAT

Abstract. The iteration of complex functions can produce captivating fractal images. The dynamical behavior of most fractals relies on escape criteria, employing diverse iterative procedures. This paper introduces a novel iterative approach known as the W-iterative method. Using this method, we initially establish escape criteria for mappings $T_1, T_2, T_3 : \mathbb{C} \to \mathbb{C}$ defined by $T_1 z = z^p + bz + c, T_2 z = z^p + qz + \log c^t, T_3 z = z^p + rz + \sin c^t$ for all $z \in \mathbb{C}$, where $p \in \mathbb{N} \setminus \{1\}$, $t \in [1, \infty)$, $b, r, q \in \mathbb{C}$ and $c \in \mathbb{C} \setminus \{0\}$. Afterward, we formulate and implement the algorithm for generating Julia sets and Mandelbrot sets. Finally, we analyze the impact of the input parameters, such as shape, size, and color, on the generated fractals through graphical and numerical experiments.

1. Introduction

Fractals, characterized by self-similar geometric patterns, are found in both natural and mathematical structures. The term "fractal," introduced by Mandelbrot in 1978 [7], has inspired applications in cryptography [4], image encryption [10,11], and data compression [6]. The study of complex iterative functions began with Julia [3] and Fatou [2], and was later formalized by Douady and Hubbard [1] through the map $\mathbb{C} \ni z \mapsto z^2 + c$, leading to the classical Julia and Mandelbrot sets. Nowadays, these ideas are defined as follows:

Definition 1.1 ([3])**.** The filled-in Julia set for $T : \mathbb{C} \to \mathbb{C}$, denoted by $\mathbb{F}_T$, is defined by $\mathbb{F}_T = \{z \in \mathbb{C} \mid \{|T^n(z)|\}_{n=0}^{\infty}$ is bounded$\}$. The set of all boundary points of $\mathbb{F}_T$ is called Julia set, denoted by $\mathbb{J}_T$.

Definition 1.2 ([8])**.** Let $T_c : \mathbb{C} \to \mathbb{C}$ is a complex-valued function such that $c \in \mathbb{C}$ is a complex parameter. The Mandelbrot set is defined as $\mathbb{M} := \{c \in \mathbb{C} :$ $\mathbb{J}_{T_c}$ is connected$\}$. Alternatively, the Mandelbrot set $\mathbb{M}$ can be defined as follows: $\mathbb{M} := \{c \in \mathbb{C} \mid T_c^n(\omega) \nrightarrow \infty$ as $n \to \infty\}$, where ω is any critical point of T_c.

The main aim of this paper is to introduce a new iterative method to establish escape criteria for the complex mappings $T_1, T_2, T_3 : \mathbb{C} \to \mathbb{C}$ defined by $T_1 z = z^p + bz + c$, $T_2 z = z^p + qz + \log c^t$, and $T_3 z = z^p + rz + \sin c^t$ for all $z \in \mathbb{C}$, where $p \in \mathbb{N} \setminus \{1\}$, $t \in [1, \infty)$, $b, r, q \in \mathbb{C}$, and $c \in \mathbb{C} \setminus \{0\}$. The proposed algorithm generates Julia and Mandelbrot sets, linking theoretical results with visual representation. Fractal characteristics such as shape, size, color, and symmetry are analyzed through

2020 *Mathematics Subject Classification.* 28A80, 37F10, 47H10, 65H10.

Key words and phrases. Julia sets, Mandelbrot sets, W-iteration, escape criterion.

The author gratefully acknowledge the financial support provided by the Faculty of Science and Technology, Contract No. SciGR 12/2568.

variations in iterative parameters and function coefficients, offering comprehensive insight into the structural and dynamic behavior of the resulting fractals.

2. Escape criteria for the novel iteration

In this section, let $T_1, T_2, T_3 : \mathbb{C} \to \mathbb{C}$ be defined by

$$T_1 z = z^p + bz + c, \quad T_2 z = z^p + qz + \log c^t, \quad T_3 z = z^p + rz + \sin c^t \tag{2.1}$$

for all $z \in \mathbb{C}$, where $p \in \mathbb{N} \setminus \{1\}$, $t \in [1, \infty)$, $b, q, r \in \mathbb{C}$, and $c \in \mathbb{C} \setminus \{0\}$. Now, we investigate the theorem for the escape criterion associated with the new iterative method $\{z_k\}_{k=0}^{\infty} \subseteq \mathbb{C}$ called W-iteration, which is defined by

$$z_{k+1} = \alpha_k T_1 z_k + \beta_k T_2 z_k + \gamma_k T_3 z_k \tag{2.2}$$

for all $k \in \mathbb{N} \cup \{0\}$, where $z_0 \in \mathbb{C}$, $\{\alpha_k\}_{k=0}^{\infty}, \{\beta_k\}_{k=0}^{\infty}, \{\gamma_k\}_{k=0}^{\infty} \subseteq (0, 1]$.

Theorem 2.1. *Let $T_1, T_2, T_3 : \mathbb{C} \to \mathbb{C}$ be defined by (2.1). Suppose that $z_0 \in \mathbb{C}$ and $\{z_k\}_{k=0}^{\infty}$ is defined by (2.2) with $\alpha_k = \alpha, \beta_k = \beta$ and $\gamma_k = \gamma$ for all $k \in \mathbb{N} \cup \{0\}$. If*

$$|z_0| \geq \max\left\{|c|, \left(\frac{2(1 + |b| + |q| + |\lambda| + |r| + |\sigma|)}{\alpha + \beta + \gamma}\right)^{\frac{1}{p-1}}\right\}, \tag{2.3}$$

where $\lambda := \frac{\log c^t}{c}, \sigma := \frac{\sin c^t}{c}$, then $\lim_{k\to\infty} |z_k| = \infty$.

Proof. From (2.2), for $k = 0$, we obtain

$$\begin{aligned}
|z_1| &= |\alpha(z_0^p + bz_0 + c) + \beta(z_0^p + qz_0 + \log c^t) + \gamma(z_0^p + rz_0 + \sin c^t)| \\
&\geq (\alpha + \beta + \gamma)|z_0|^p - \alpha|b||z_0| - \alpha|c| - \beta|q||z_0| - \beta|c||\lambda| - \gamma|r||z_0| - \gamma|c||\sigma| \\
&\geq (\alpha + \beta + \gamma)|z_0|^p - \alpha|b||z_0| - \alpha|z_0| - \beta|q||z_0| - \beta|z_0||\lambda| - \gamma|r||z_0| - \gamma|z_0||\sigma| \\
&= |z_0|\big[(\alpha + \beta + \gamma)|z_0|^{p-1} - (\alpha + \alpha|b| + \beta|q| + \beta|\lambda| + \gamma|r| + \gamma|\sigma|)\big] \\
&\geq |z_0|\big[(\alpha + \beta + \gamma)|z_0|^{p-1} - (1 + |b| + |q| + |r| + |\lambda| + |\sigma|)\big].
\end{aligned}$$

The condition (2.3) yields

$$(\alpha + \beta + \gamma)|z_0|^{p-1} - [1 + |b| + |q| + |r| + |\lambda| + |\sigma|] \geq 1 + |b| + |q| + |r| + |\lambda| + |\sigma|.$$

From the last two reults, we have $|z_1| \geq (1 + |b| + |q| + |r| + |\lambda| + |\sigma|)|z_0| \geq |z_0|$. This yields that

$$|z_1| \geq \max\left\{|c|, \left(\frac{2(1 + |b| + |q| + |\lambda| + |r| + |\sigma|)}{\alpha + \beta + \gamma}\right)^{\frac{1}{p-1}}\right\}.$$

Therefore, $|z_1|$ satisfies the same condition as $|z_0|$. By applying the same process with $k = 0$, we obtain the result for $k = 1$ as follows:

$$|z_2| \geq (1 + |b| + |q| + |r| + |\lambda| + |\sigma|)^2 |z_0|.$$

After k^{th}-steps, we get

$$|z_k| \geq (1 + |b| + |q| + |r| + |\lambda| + |\sigma|)^k |z_0|.$$

It follows from $1 + |b| + |q| + |r| + |\lambda| + |\sigma| > 1$ that $\lim_{k\to\infty} |z_k| = \infty$. □

By applying Theorem 2.1, the ensuing corollary emerges as follows:

Corollary 2.2. *Let $T_1, T_2, T_3 : \mathbb{C} \to \mathbb{C}$ be defined by (2.1). Suppose that $z_0 \in \mathbb{C}$ and $\{z_k\}_{k=0}^{\infty}$ is defined by (2.2) with $\alpha_k = \alpha, \beta_k = \beta$ and $\gamma_k = \gamma$ for all $k \in \mathbb{N} \cup \{0\}$. If*

$$|z_j| \geq \max\left\{|c|, \left(\frac{2(1+|b|+|q|+|\lambda|+|r|+|\sigma|)}{\alpha+\beta+\gamma}\right)^{\frac{1}{p-1}}\right\}$$

for some $j \in \mathbb{N} \cup \{0\}$, where $\lambda := \frac{\log c^t}{c}, \sigma := \frac{\sin c^t}{c}$, then $\lim_{k\to\infty} |z_k| = \infty$.

Remark 2.3. Corollary 2.2 provides the escape radius

$$R := \max\left\{|c|, \left(\frac{2(1+|b|+|q|+|r|+|\lambda|+|\sigma|)}{\alpha+\beta+\gamma}\right)^{\frac{1}{p-1}}\right\}.$$

If $|z_j| > R$ for some $j \in \mathbb{N} \cup \{0\}$, then $\{|z_k|\}_{k=0}^{\infty}$ diverges to infinity and thus lies outside the region corresponding to the Julia and Mandelbrot sets. Consequently, any point located beyond the circle centered at the origin with radius R is not contained in these sets, while only the points within this circle belong to them.

3. Generation of fractals

In this section, Algorithms 1 and 2 were implemented in MATLAB R2021a to generate the Julia and Mandelbrot sets. All computations were performed on a system equipped with an AMD Ryzen 5 7520U (2.80 GHz) processor and 8 GB RAM under Windows 11 (64-bit). For visualization, the standard "jet" colormap was applied to color the data points, as shown in Figure 1.

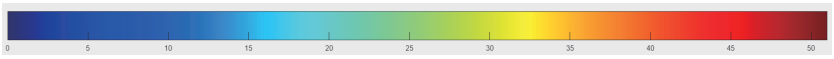

Figure 1. A colormap is used in Section 3.

Algorithm 1: Creating Julia Set

Input: $T_1, T_2, T_3 : \mathbb{C} \to \mathbb{C}$-mappings defined by (2.1); $U \subseteq \mathbb{C}$-considered region; K-maximum number of iterations; $\alpha, \beta, \gamma \in (0, 1]$-parameters of the W-iterative method; $[0..M]$-colormap with $M + 1$ colors

Output: Julia set for U

$\lambda = \frac{\log(c^t)}{c}$, $\sigma = \frac{\sin(c^t)}{t}$, $R = \max\left\{|c|, \left(\frac{2(1+\alpha|b|+\beta|q|+|\lambda|+\gamma|\sigma|+\gamma|r|)}{\alpha+\beta+\gamma}\right)^{\frac{1}{p-1}}\right\}$

for $z_0 \in U$ **do**

  $k = 0$

  while $k < K$ *and* $|z_k| \leq R$ **do**

    $z_{k+1} = \alpha T_1 z_k + \beta T_2 z_k + \gamma T_3 z_k$

    $k = k + 1$

  $i = \lfloor M\frac{k}{K} \rfloor$

  color z_0 with color map $[i]$

Algorithm 2: Creating Mandelbrot set

Input: $T_1, T_2, T_3 : \mathbb{C} \to \mathbb{C}$-mappings defined by (2.1); $U \subseteq \mathbb{C}$-considered region; K-maximum number of iterations; $\alpha, \beta, \gamma \in (0, 1]$-parameters of the W-iterative method; $[0..M]$-colormap with $M + 1$ colors

Output: Mandelbrot set for U

for $c \in U$ **do**
  if $c = 0$ **then**
    discard the point
  $\lambda = \frac{\log c^t}{c}, \sigma = \frac{\sin c^t}{t}$, $R = \max\left\{|c|, \left(\frac{2(1+\alpha|b|+\beta|q|+|\lambda|+\gamma|\sigma|+\gamma|r|)}{\alpha+\beta+\gamma}\right)^{\frac{1}{p-1}}\right\}$
  $k = 0$, $z_0 = c$
  while $k < K$ *and* $|z_k| \leq R$ **do**
    $z_{k+1} = \alpha T_1 z_k + \beta T_2 z_k + \gamma T_3 z_k$
    $k = k + 1$
  $i = \lfloor M \frac{k}{K} \rfloor$
  color c with color map $[i]$

3.1. **Julia sets.** In Algorithm 1, the Julia set is generated with a maximum of 50 iterations over the region $U = [-1.5, 1.5] \times [-1.5, 1.5]$ in the complex plane. Parameters are initialized as $b = i$, $q = 0.2$, $r = 0.3$, $c = -0.06$, $\alpha = 0.01$, $\beta = 0.11$, $\gamma = 0.98$, $t = 6$, and $p = 2$, each varied individually to study its effect on the set's shape, size, and color.

Figure 2 shows quadratic Julia sets for different integer values of t. For $t < 4$, the sets are rotationally symmetric but not with respect to the axes. As t increases, they contract and elongate along the real axis with reduced brown intensity, giving the most aesthetic pattern at $t = 3$. Figure 3 illustrates sets for non-integer $t \in (4, 5)$, where twisting patterns appear; increasing t slightly reduces size while enhancing the brown hue.

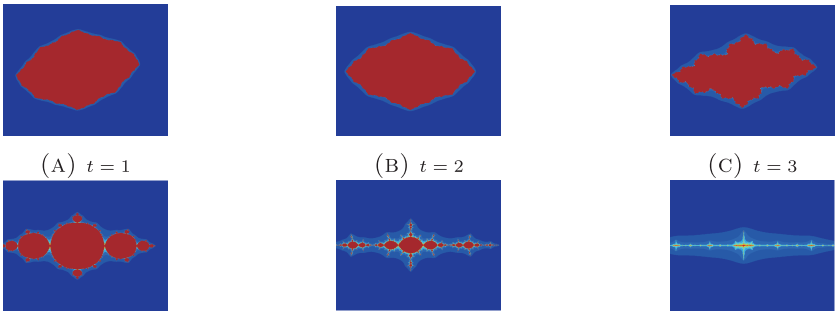

(A) $t = 1$ (B) $t = 2$ (C) $t = 3$

(D) $t = 5$ (E) $t = 6$ (F) $t = 9$

FIGURE 2. Effect of varying the integer parameter t.

Figure 4 illustrates quadratic Julia sets obtained by varying c. As the real part of c increases, the sets expand and display stronger brown coloration. For a small

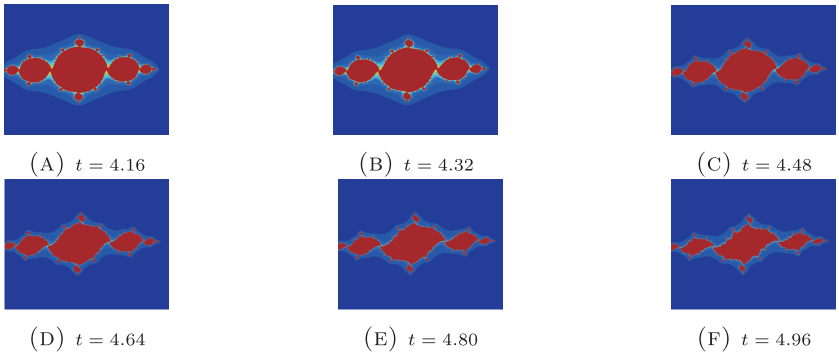

FIGURE 3. Effect of varying the non-integer parameter t.

positive real c, the sets appear disconnected. When c is complex with $|c| \approx 1$, the sets are faint and fragmented, whereas for very small $|c|$, they enlarge, exhibit higher color intensity, and reveal subtle yellow and sky-blue edges. In all cases, the sets are predominantly elongated along the real axis.

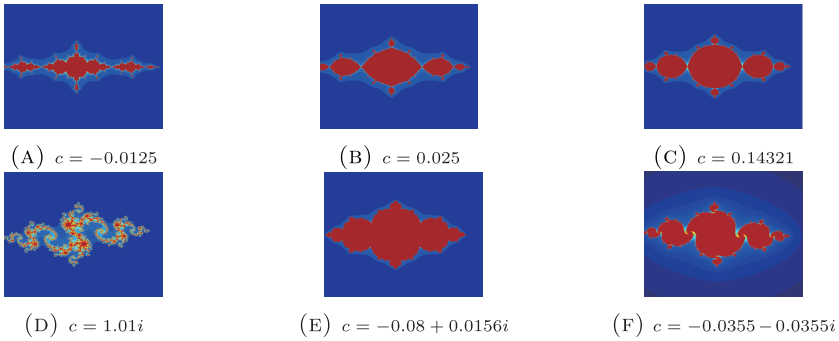

FIGURE 4. Effect of varying the parameter c.

Figure 5 displays quadratic Julia sets generated by varying b. All sets exhibit symmetry and elongation along the real axis, regardless of whether b is real or complex. Changes in b produce only minor differences in the size, shape, and color of the Julia sets.

Figure 6 shows quadratic Julia sets for varying q. For real q, larger magnitudes expand the sets and deepen the brown tone while fading the sky-blue and yellow hues. For complex q, the sets split into a central region with two twisted side parts, all remaining elongated along the real axis.

Figure 7 shows quadratic Julia sets for different r. As r increases from negative to positive, the sets expand, the brown tones deepen, and the sky-blue hues fade. For complex r, small positive parts preserve symmetry about the real axis, while negative parts break it, fading brown shades, enhancing blue areas, and yielding smaller disconnected forms.

Figure 8 shows quadratic Julia sets for various α. Smaller α enlarges the sets and darkens the brown color, while larger α makes them smaller, stretched along the real axis, and shifts hues toward sky-blue. Around $\alpha = 0.5$ disconnections occur,

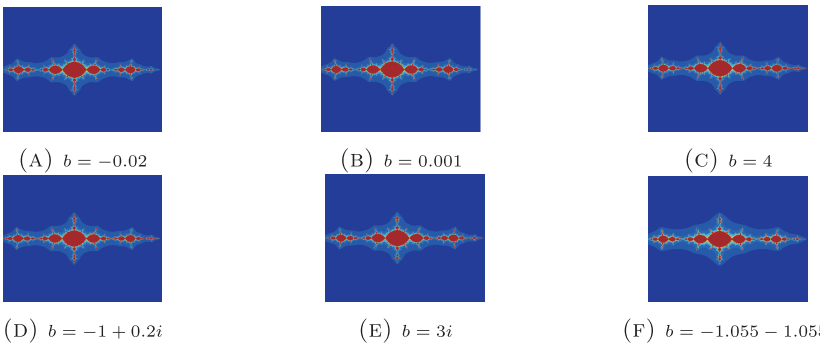

FIGURE 5. Effect of varying the parameter b.

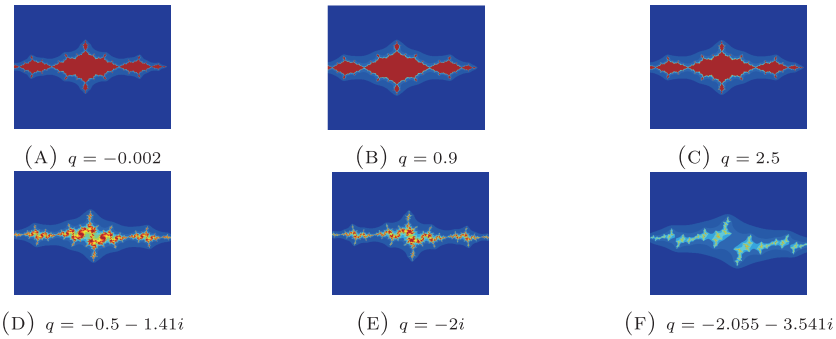

FIGURE 6. Effect of varying the parameter q.

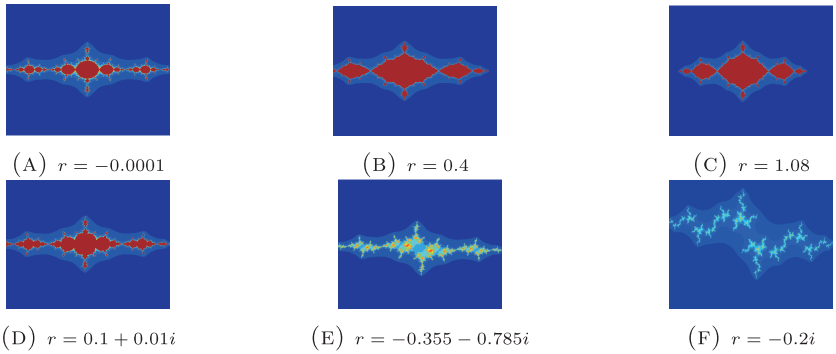

FIGURE 7. Effect of varying the parameter r.

and near $\alpha = 1$ more points escape, reflecting the strong effect of α on size and stability.

Figure 9 shows Julia sets for different β values. When β is near zero, the sets enlarge and flatten along the imaginary axis. Increasing β contracts and stretches them along the real axis, while the brown tone fades. For $\beta \geq 0.4$, the inner region divides into two sky-blue parts with small yellow substructures that separate further as β approaches one, causing more points to escape the region.

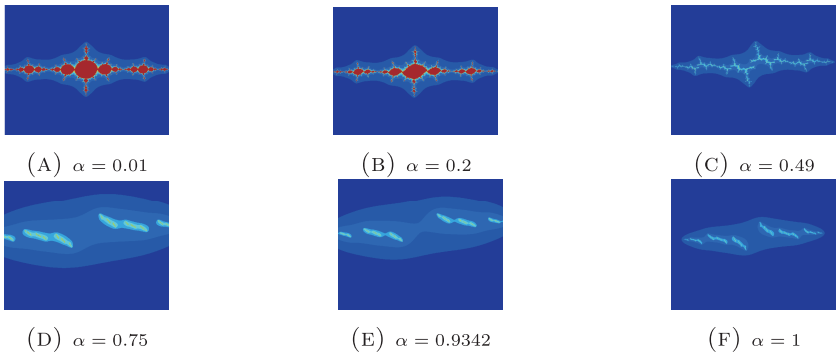

(A) $\alpha = 0.01$ (B) $\alpha = 0.2$ (C) $\alpha = 0.49$

(D) $\alpha = 0.75$ (E) $\alpha = 0.9342$ (F) $\alpha = 1$

FIGURE 8. Effect of varying the parameter α.

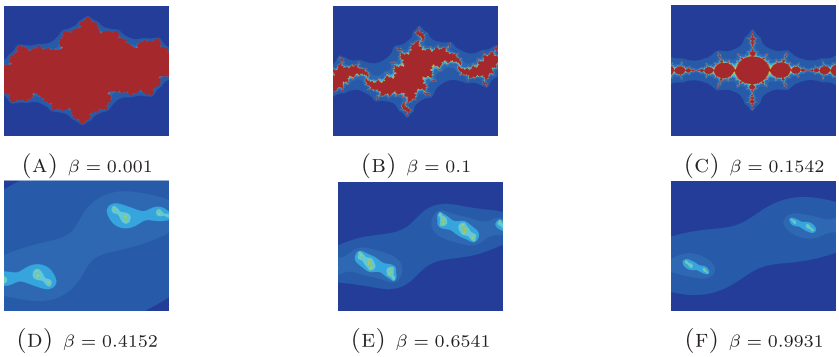

(A) $\beta = 0.001$ (B) $\beta = 0.1$ (C) $\beta = 0.1542$

(D) $\beta = 0.4152$ (E) $\beta = 0.6541$ (F) $\beta = 0.9931$

FIGURE 9. Effect of varying the parameter β.

Figure 10 depicts Julia sets for different values of γ. When γ is near zero, the sets expand and appear flattened. As γ increases, they become smaller and more elongated along the real axis. For γ greater than or equal to 0.6, the sets separate into three regions around the real axis, consisting of one large central part and two smaller side parts.

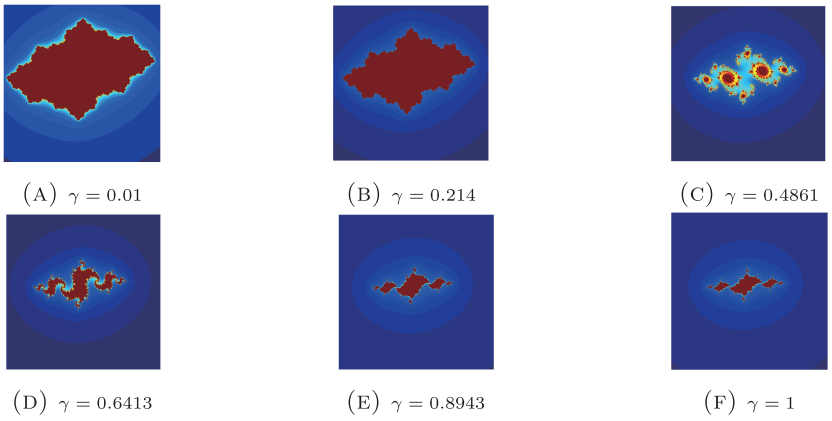

(A) $\gamma = 0.01$ (B) $\gamma = 0.214$ (C) $\gamma = 0.4861$

(D) $\gamma = 0.6413$ (E) $\gamma = 0.8943$ (F) $\gamma = 1$

FIGURE 10. Effect of varying the parameter γ.

Figure 11 shows Julia sets for fixed parameters $c = -0.06$, $t = 6$, $\alpha = 0.51$, $\beta = 0.11$, $\gamma = 0.95$, $b = i$, $q = 0.2$, and $r = 0.3$, with varying p. Except for $p = 3$, all sets remain symmetric about the real axis. Odd p values produce sky-blue, multi-lobed patterns, while even $p \leq 18$ yield mainly brown forms with small peripheral parts. For large p, the boundary becomes circular and the inner pattern grows more intricate.

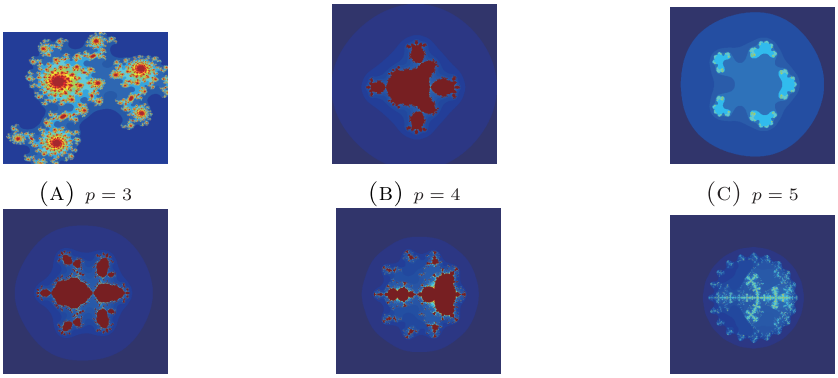

(A) $p = 3$ (B) $p = 4$ (C) $p = 5$

(D) $p = 6$ (E) $p = 10$ (F) $p = 20$

FIGURE 11. Effect of varying the parameter p.

3.2. **Mandelbrot sets.** Mandelbrot sets are generated using Algorithm 2 with $K = 50$ iterations over $U = [-3, 3] \times [-3, 3]$, fixing $b = 0.2$, $r = 0.03$, $q = 0.1$, $\alpha = 0.05$, $\beta = 0.21$, $\gamma = 0.001$, $t = 6$, and $p = 2$, while varying each parameter individually to observe structural changes. Figures 12 and 13 show sets for integer and non-integer t. For integer t, they are axis-symmetric—large and round at $t = 1$ with brown centers and thin yellow-blue rims; as t increases, the brown fades and $2t$ narrow lashes form. For non-integer t, symmetry breaks along the imaginary axis, producing thinner, less distinct lashes.

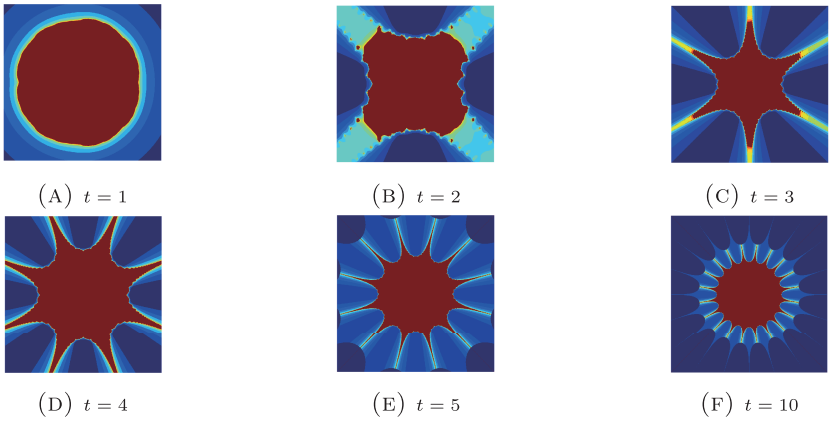

(A) $t = 1$ (B) $t = 2$ (C) $t = 3$

(D) $t = 4$ (E) $t = 5$ (F) $t = 10$

FIGURE 12. Effect of varying the integer parameter t.

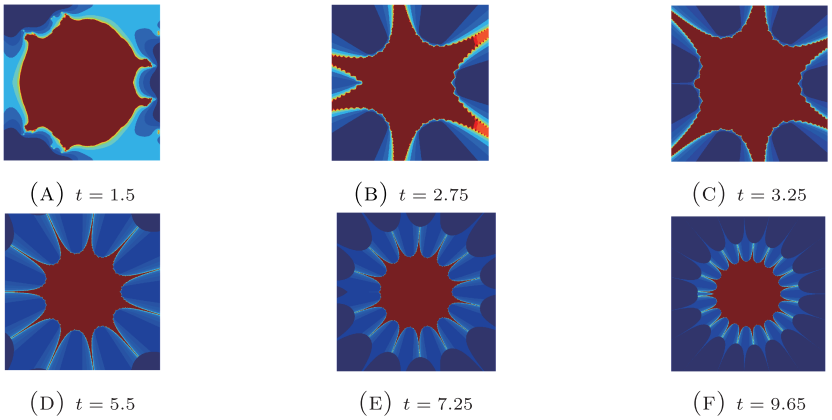

(A) $t = 1.5$ (B) $t = 2.75$ (C) $t = 3.25$

(D) $t = 5.5$ (E) $t = 7.25$ (F) $t = 9.65$

FIGURE 13. Effect of varying the non-integer parameter t

As shown in Figure 14, changing b (real or complex) produces no significant differences in size, shape, or color. All sets remain symmetric and primarily brown.

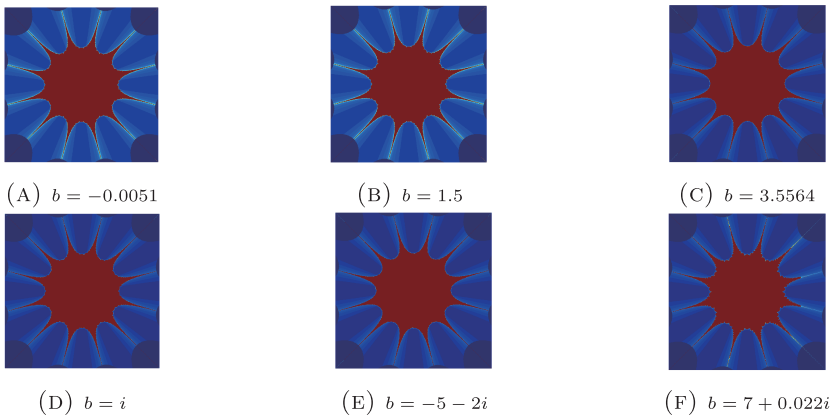

(A) $b = -0.0051$ (B) $b = 1.5$ (C) $b = 3.5564$

(D) $b = i$ (E) $b = -5 - 2i$ (F) $b = 7 + 0.022i$

FIGURE 14. Effect of varying the parameter b.

Figure 15 shows that altering r does not affect the main structure. All sets display a brown tone with about twelve lashes against a blue background.

As shown in Figure 16, increasing real q reduces the Mandelbrot set's size, with yellow-blue shades emerging near the right side. For complex q with negative parts, the set appears uniformly brown. When both parts are positive and large, the set turns entirely sky-blue, and the right inner region vanishes.

Figure 17 shows that for small α, the Mandelbrot set is large, symmetric, and brown. As α increases, symmetry fades, and the right inner part shrinks. The brown color weakens and transitions to yellow and sky-blue, while near $\alpha = 1$, fragmentation occurs.

As shown in Figure 18, the Mandelbrot sets remain symmetric for all β. For small β, the sets are mainly brown. Increasing β reduces the size and introduces six lashes near $\beta = 0.57$. Beyond $\beta \geq 0.7$, the sets fragment into six smaller parts.

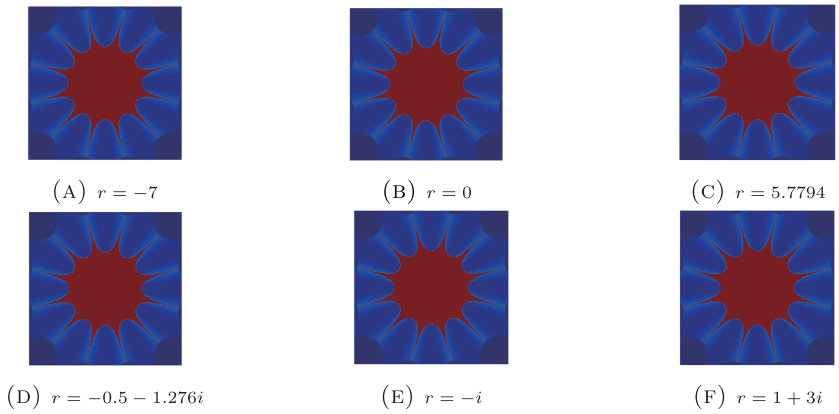

(A) $r = -7$ (B) $r = 0$ (C) $r = 5.7794$

(D) $r = -0.5 - 1.276i$ (E) $r = -i$ (F) $r = 1 + 3i$

FIGURE 15. Effect of varying the parameter r.

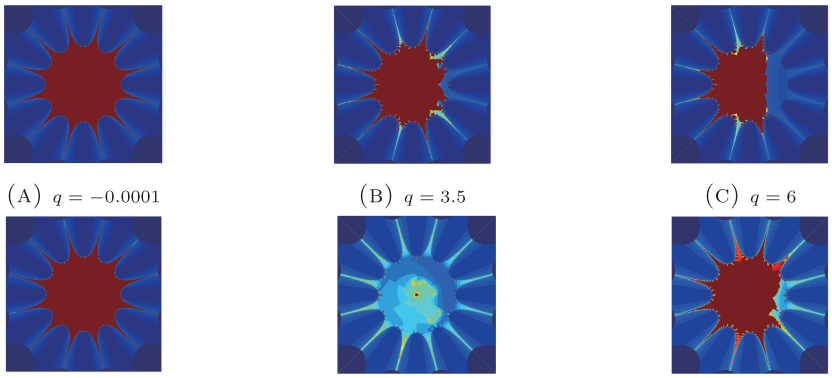

(A) $q = -0.0001$ (B) $q = 3.5$ (C) $q = 6$

(D) $q = -1 - 3i$ (E) $q = 5 + 6.76i$ (F) $q = 4 - 0.5i$

FIGURE 16. Effect of varying the parameter q.

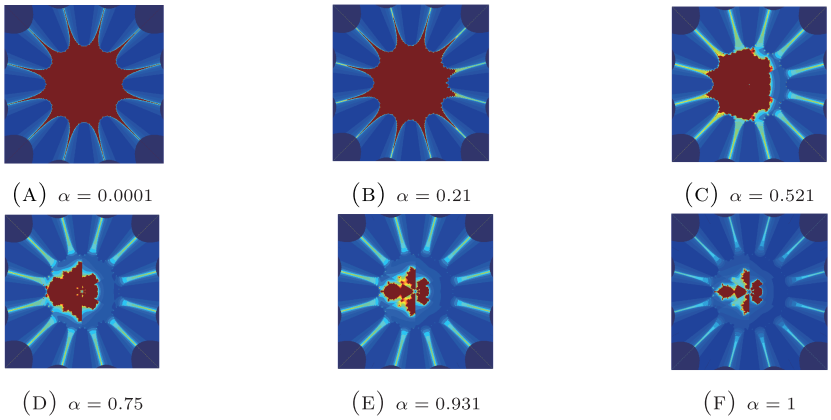

(A) $\alpha = 0.0001$ (B) $\alpha = 0.21$ (C) $\alpha = 0.521$

(D) $\alpha = 0.75$ (E) $\alpha = 0.931$ (F) $\alpha = 1$

FIGURE 17. Effect of varying the parameter α.

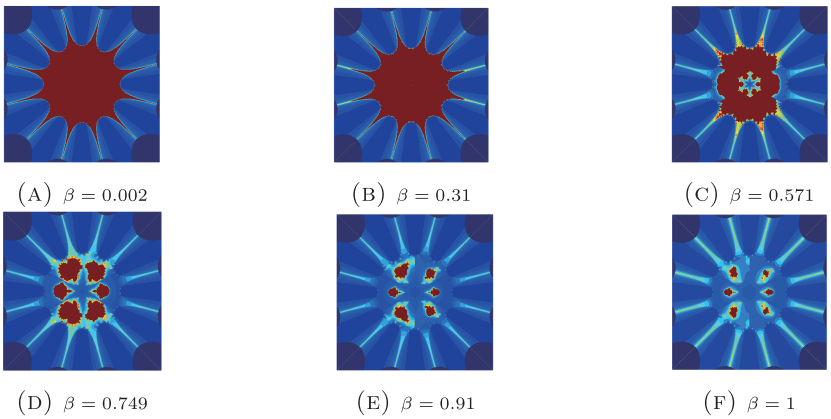

(A) $\beta = 0.002$ (B) $\beta = 0.31$ (C) $\beta = 0.571$

(D) $\beta = 0.749$ (E) $\beta = 0.91$ (F) $\beta = 1$

FIGURE 18. Effect of varying the parameter β.

Figure 19 demonstrates that as γ increases, the inner region shrinks and becomes distorted. Brown lashes disappear, forming a rectangular core with six yellow-blue lashes. The outer lashes remain constant across all γ values.

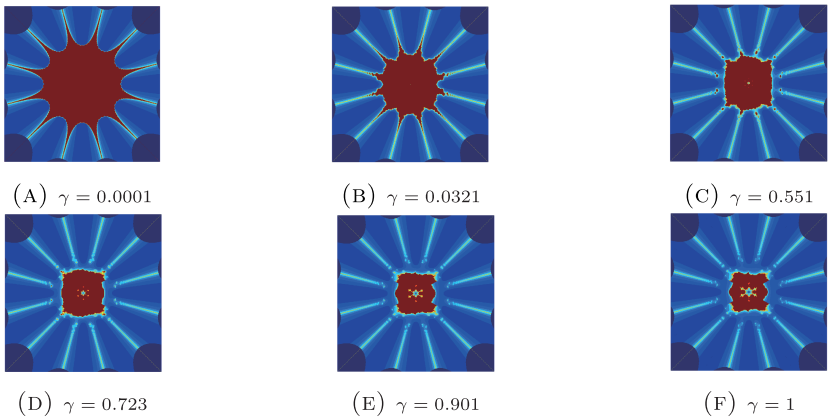

(A) $\gamma = 0.0001$ (B) $\gamma = 0.0321$ (C) $\gamma = 0.551$

(D) $\gamma = 0.723$ (E) $\gamma = 0.901$ (F) $\gamma = 1$

FIGURE 19. Effect of varying the parameter γ on the Mandelbrot sets.

As shown in Figure 20, increasing p decreases the size of the brown inner lashes and makes the inner region circular. Beyond $p = 3$, a new structure with t lashes appears at the center. The outer lashes remain unchanged, but their hue gradually shifts with increasing p.

4. Numerical results

This section numerically examines Julia and Mandelbrot sets generated by the W-iteration method, analyzing structural and computational changes under parameter variation. Two metrics are considered [5, 9]: generation time for efficiency and average number of iterations (ANI) for fractal complexity. All computations were

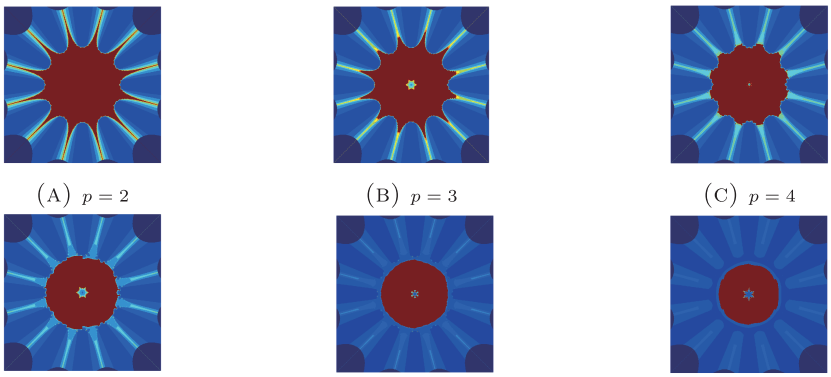

(A) $p = 2$ (B) $p = 3$ (C) $p = 4$

(D) $p = 5$ (E) $p = 6$ (F) $p = 10$

FIGURE 20. Effect of varying the parameter p on the Mandelbrot sets.

done in MATLAB R2021a on an AMD Ryzen 5 7520U (8 GB RAM, Windows 11, 64-bit) using 400×400 resolution with one parameter varied at a time.

4.1. **Julia sets.** The Julia sets were generated using Algorithm 1 with parameters $b = i$, $q = 0.2$, $r = 0.3$, $c = -0.06$, $\alpha = 0.51$, $\beta = 0.11$, $\gamma = 0.5$, $t = 6$, and $p = 2$, over the region $U = [-2, 2] \times [-2, 2] \subseteq \mathbb{C}$. Figures 21 and 22 show that both computation time and ANI decrease as α, β, γ, and t increase, implying faster convergence and simpler fractal geometry. Notably, β exhibits a sharp initial drop before stabilizing, while t shows a brief complexity peak before settling, reflecting transitional changes in the fractal's structural dynamics and computational efficiency.

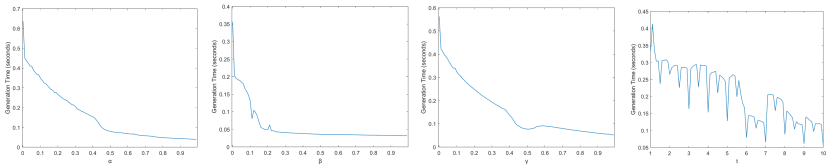

(A) Varying α (B) Varying β (C) Varying γ (D) Varying t

FIGURE 21. Execution time variations for different parameters α, β, γ, and t in Julia set generation.

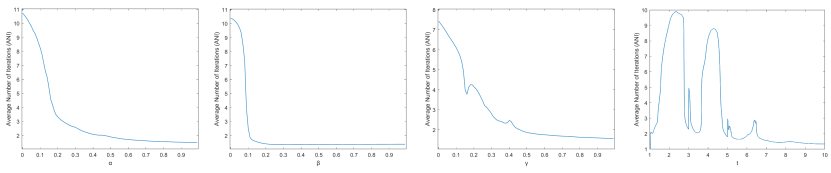

(A) Varying α (B) Varying β (C) Varying γ (D) Varying t

FIGURE 22. ANI variations for parameters α, β, γ, and t.

4.2. **Mandelbrot sets.** The Mandelbrot sets were generated using Algorithm 2 with parameters $p = 2$, $\beta = 0.21$, $\gamma = 0.001$, $t = 6$, $b = 0.2$, $r = 0.03$, $q = 0.1$, and $\alpha \in (0, 1]$, over the region $A = [-3, 3] \times [-3, 3] \subseteq \mathbb{C}$. Figures 23 and 24 show the variations in computation time and Average Number of Iterations (ANI) as α, β, γ, and t change.

As observed in Figure 23, the computation time generally decreases with increasing parameter values, reflecting faster convergence of the iteration process. Figure 24 demonstrates that ANI follows a similar pattern, suggesting smaller and less intricate fractal structures for larger parameter values. However, β shows a pronounced drop beyond $\beta > 0.3$, while t exhibits a steady decline after a short plateau, indicating a shift in escape dynamics and overall fractal density.

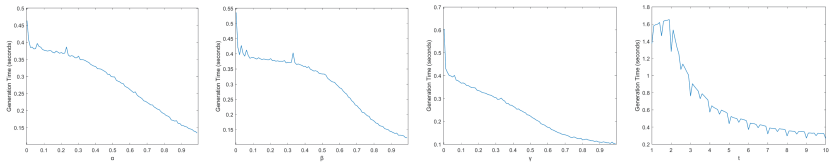

(A) Varying α (B) Varying β (C) Varying γ (D) Varying t

FIGURE 23. Execution time variations for different parameters α, β, γ, and t in Mandelbrot set generation.

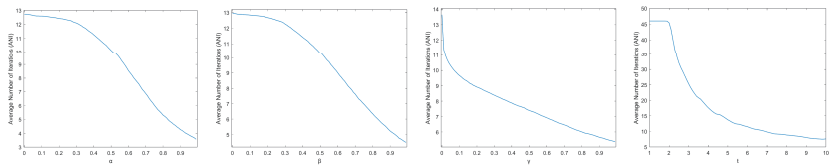

(A) Varying α (B) Varying β (C) Varying γ (D) Varying t

FIGURE 24. ANI variations for parameters α, β, γ, and t in Mandelbrot set generation.

5. Conclusions

This study introduced the W-iteration scheme as a new iterative approach and established corresponding escape criteria for complex-valued mappings defined by (2.1). The method effectively generates diverse Julia and Mandelbrot sets, revealing rich geometric structures and color transitions influenced by parameters α, β, γ, t, b, r, q, and p. Numerical findings demonstrate that increasing the iterative parameters enhances computational efficiency while simplifying fractal geometry, whereas smaller values yield more intricate and aesthetically detailed patterns. The results confirm that the W-iteration provides a unified framework connecting theoretical fixed-point concepts with the computational generation and visual analysis of complex fractal dynamics.

References

[1] A. Douady and J. Hubbard, *Iteration des polynômes quadratiques complexes*, C. R. Acad. Sci. Paris Sér. I Math. **294** (1982), 123–126.

[2] P. Fatou, *Sur les substitutions rationnelles*, C. R. Acad. Sci. Paris **164** (1917), 806–808.

[3] G. Julia, *Mémoire sur l'itération des fonctions rationnelles*, J. Math. Pures Appl. **8** (1918), 47–74.

[4] S. Kumar, *Public key cryptographic system using Mandelbrot sets*, in: MILCOM 2006 - 2006 IEEE Military Communications conference, Washington, DC, USA, 2006, pp. 1–5.

[5] S. Kumari, K. Gdawiec, A. Nandal, M. Postolache and R. Chugh, *A novel approach to generate Mandelbrot sets, Julia sets and biomorphs via viscosity approximation method*, Chaos Solitons Fractals **163** (2022): 112540.

[6] S. Liu, W. Bai, G. Liu, W. Li and H. Srivastava, *Parallel fractal compression method for big video data*, Complexity **2018** (2018): 2016976.

[7] B. B. Mandelbrot, *Fractals: Form, Chance, and Dimension*, Freeman, 1977.

[8] B. B. Mandelbrot, *The Fractal Geometry of Nature*, W. H. Freeman, New York, 1982.

[9] A. Shahid, W. Nazeer and K. Gdawiec, *The Picard–Mann iteration with s-convexity in the generation of Mandelbrot and Julia sets*, Monatshefte für Mathematik **195** (2021), 565–584.

[10] Y. Sun, L. Chen, R. Xu and R. Kong, *An image encryption algorithm utilizing Julia sets and Hilbert curves*, PLOS ONE **9** (2014): e84655.

[11] X. Zhang, L. Wang, Z. Zhou and Y. Niu, *A chaos-based image encryption technique utilizing Hilbert curves and H-fractals*, IEEE Access **7** (2019), 74734–74746.

Manuscript received March 8, 2025
revised October 2, 2025

N. Adhikari
Central Department of Mathematics, Faculty of Science and Technology, Tribhuvan University, Nepal
E-mail address: nabaraj.adhikari@cdmath.tu.edu.np

W. Sintunavarat
Department of Mathematics and Statistics, Faculty of Science and Technology, Thammasat University Rangsit Center, Pathum Thani 12120, Thailand
E-mail address: wutiphol@mathstat.sci.tu.ac.th